Polymer Chemistry

rsc.li/polymers

RAFT

PAPER

Prokopios Georgopanos, Volker Abetz *et al.*
Well-defined polyvinylpyridine-*block*-polystyrene diblock copolymers *via* RAFT aqueous-alcoholic dispersion polymerization: synthesis and isoporous thin film morphology

ROYAL SOCIETY OF CHEMISTRY

Check for updates

Well-defined polyvinylpyridine-*block*-polystyrene diblock copolymers *via* RAFT aqueous-alcoholic dispersion polymerization: synthesis and isoporous thin film morphology†

Katharina Nieswandt, [ID] [a] Prokopios Georgopanos [ID] *[a] and Volker Abetz [ID] *[a,b]

In this work, the synthesis and characterization of polyvinylpyridine-polystyrene (PVP-*b*-PS) diblock copolymers *via* reversible addition–fragmentation chain transfer (RAFT) dispersion polymerization is presented. A series of poly(4-vinylpyridine) (P4VP) and poly(2-vinylpyridine) (P2VP) homopolymers were prepared by RAFT bulk polymerization at 80 °C using either a carboxylic acid functionalized trithiocarbonate or a non-functionalized trithiocarbonate RAFT agent. The P4VP and P2VP macroRAFT agents acted as stabilizers in the subsequent RAFT-mediated polymerization-induced self-assembly (PISA), when they were chain extended *via* RAFT aqueous-alcoholic dispersion polymerization of styrene at 70 °C. Following this protocol, high styrene conversions between 86–99% were achieved, leading to a series of well-defined, high molecular weight PVP-*b*-PS diblock copolymers with narrow molecular weight distributions as confirmed by proton nuclear magnetic resonance (¹H NMR) spectroscopy and gel permeation chromatography (GPC). The bulk and surface morphologies of the diblock copolymers were investigated *via* transmission electron microscopy (TEM), atomic force microscopy (AFM), and scanning electron microscopy (SEM). The solution-cast and spin-coated thin films of the P4VP-*b*-PS and P2VP-*b*-PS diblock copolymers exhibited microphase-separated structures with spherical or cylindrical order according to their compositions. Spin-coated PVP-*b*-PS diblock copolymer films with weight fractions of the minority PVP block ranging from 17–24% were converted into porous surfaces by a controlled alignment and swelling strategy, exploiting the distinct selectivities of different solvents for the individual blocks.

Introduction

Over the past decades, controlled reversible deactivation radical polymerization (RDRP) has been developed into a versatile and widely used technique to synthesize well-defined polymers.[1–3] Nowadays, it is an established method of choice to design precisely structured block copolymers *via* radical polymerization.[4,5] Initially, RDRP techniques, including the extensively studied atom transfer radical polymerization (ATRP), nitroxide-mediated polymerization (NMP) and reversible addition–fragmentation chain transfer (RAFT) polymerization, were conducted as homogeneous polymerizations in bulk, organic solvents, or water.[6–8] Although such polymeriz-

ations are still of high interest today, the well-controlled polymerization of slowly-propagating radicals, such as resonance-stabilized styrenics, appeared challenging for decades.[9] Since a long time, polystyrene latexes are produced mostly by free radical heterogeneous polymerizations stabilized and controlled by surfactants as emulsifiers.[10–12] Those polymer colloids dispersed in aqueous systems are formed by free radical emulsion (or 'latex') polymerizations.[13] Commonly, they are stabilized by a surfactant, which stabilizes the emulsion at the beginning and the monomer-swollen micelles as well as the latex particles towards the end of the polymerization.[7,14] However, on the one hand, surfactants may separate from the particles, which may lead to particle coagulation. On the other hand, it is difficult to remove the surfactant completely from the final polymer. Surfactant-free emulsion polymerization systems were developed in the 1970s in order to avoid the adverse side effects that arose from surfactant-controlled emulsion polymerizations.[15] This polymerization technique, which gained importance during the Second World War, has developed into a global industry.[13] Nowadays, the combination of RDRP methods with emulsion or dispersion polymerization

[a]Helmholtz-Zentrum Geesthacht, Institute of Membrane Research, Max-Planck-Straße 1, 21502 Geesthacht, Germany. E-mail: prokopios.georgopanos@hzg.de, volker.abetz@hzg.de
[b]Institute of Physical Chemistry, University of Hamburg, Martin-Luther-King-Platz 6, 20146 Hamburg, Germany

techniques is a feasible approach to produce research and industrially relevant copolymers with predetermined molecular weights and architectures.[16,17] These methods provide efficient heat transfer, low viscosity during the entire reaction time and enable the production of well-defined polymers.[14,16–18]

Dispersion polymerization initially involves a completely homogeneous solution.[19–22] However, the resultant polymer is not soluble in the polymerization medium.[7,23] In RAFT dispersion polymerization, a previously synthesized soluble homopolymer, a so-called macromolecular chain transfer agent (macroRAFT agent), is used as the stabilizer of the following dispersion polymerization. Initially, the second block grows continuously in the homogenous phase. With increasing length of the second block, the forming amphiphilic diblock copolymer chains become increasingly insoluble in the reaction medium. Once a critical block length exceeds the critical micelle degree of polymerization (CMDP), the amphiphilic diblock copolymers self-assemble into sterically stabilized spherical micelles.[7] This phase separation process is called polymerization-induced self-assembly (PISA) and is caused by the insolubility of the second block in the polymerization medium during the continuous chain extension.[24–28] Especially for the commonly slow polymerization of monomers like styrene,[29] PISA has proven to be a viable approach to accelerate RAFT polymerizations.[30–32] Over the years, PISA has evolved into a versatile technique for the efficient synthesis of block copolymer nanoparticles.[33–36] In recent years, numerous polymerization protocols for aqueous emulsions, aqueous dispersions or non-aqueous polymerizations have been developed. In particular, RAFT formulations in alcoholic media have received considerable attention.[37–39] PISA formulations in pure alcoholic media often showed incomplete monomer conversions and slow reaction rates. Several research groups investigated the influence of water, as co-solvent, on alcoholic PISA formulations. Charleux et al. studied the polymerization of benzyl methacrylate (BzMA) in dispersion polymerizations when using a poly(methacrylic acid-co-poly(ethylene oxide) monomethyl ether methacrylate) (P(MAA-b-PEOMA)) macroRAFT agent.[40] Similarly, Zhang et al. investigated the dispersion polymerization of styrene in ethanol/water using a 2-(dodecylthiocarbonothioylthio)-2-methylpropionic acid (BDMAT) RAFT agent.[41] Their results showed that the use of water as co-solvent in alcoholic media significantly increased the polymerization rates. Based on these findings, Armes et al. examined the chain extension of poly(2-(dimethylamino)ethyl methacrylate) (PDMA) macroRAFT agent with benzyl methacrylate (BzMA) in ethanol/water mixtures and also found a significant increase in reaction rates.[42] They attributed this increase to the insolubility of the monomer in water, which then preferentially enters the growing particles, increasing the local monomer concentration and thus increasing the rate of polymerization.[40,42] Furthermore, water as a co-solvent reduces the solubility of the growing polymer chains, which lowers the CMDP. The initial (slow) homogeneous polymerization turns more rapidly into a faster dispersion polymerization.[40–42]

During the past years, there has been a growing interest in nanostructured materials for technological applications, such as nanostructured membranes, templates and data storage media. Amongst others, near-monodisperse diblock copolymers, which consist of two incompatible blocks, were brought into focus.[43–47] Sriprom et al. studied the microphase separation of diblock copolymers synthesized via RAFT polymerization, containing one monodisperse (poly(methyl methacrylate) (PMMA) block and one polydisperse (poly(butyl acrylate) (PBA) block, in thin films.[48] The PMMA-b-PBA diblock copolymers microphase-separated into regularly ordered domains with high reproducibility and long-range order. However, they observed that an increase in dispersity led to a shift of the morphological transitions to more asymmetric volume fractions, in comparison to a monodisperse system. Essentially the same observations were previously reported by Hillmyer and co-workers.[49] Their predictions suggested that the domain spacing increased as the dispersity of one block was increased, while the dispersity of the other block remained constantly narrow.

In order to control the orientation of the block copolymer microdomains precisely, numerous techniques have been developed.[50–53] Especially methods that rely on external stimuli are important since they do not alter the chemistry of the block copolymer components on a molecular level.[54] External constraints that eliminate orientational and topological defects of self-assembled block copolymers could be temperature gradients, solvent annealing or shear.[55] In particular, extensively studied solvent vapor annealing presents an effective and non-destructive way to influence the orientation of block copolymer microdomains in thin films.[47,51,56,57]

A convenient approach to synthesize medium molecular weight poly(3-vinylpyridine)-b-polystyrene via RAFT emulsion polymerization and their thin film morphology were presented before.[18] In the present study, poly(4-vinylpyridine) (P4VP) and poly(2-vinylpyridine) (P2VP) were employed as macroRAFT agents. Here, a two-step synthetic route to poly(4-vinylpyridine)-b-polystyrene and poly(2-vinylpyridine)-b-polystyrene is described via a RAFT aqueous-alcoholic dispersion polymerization, which takes advantage of the PISA approach. The first block contains 4VP or 2VP polar moieties, which are expected to stabilize the dispersion polymerization and to enable PISA. The two isomers P2VP and P4VP are characterized in their chemical behavior by the functionality of nitrogen within the aromatic system.[58] Simple alcohols such as methanol tend to dissolve both isomers quite well due to the formation of hydrogen bonds, whereas polystyrene is not dissolved in common alcohols. The RAFT dispersion polymerization used in this work takes advantage of these different solubilities. The trithiocarbonate terminated P4VP/P2VP block is synthesized via RAFT bulk polymerization in the first step at 80 °C, followed by a surfactant-free RAFT dispersion polymerization of styrene at 70 °C in an 80 : 20 methanol/water mixture. For this purpose, either a carboxylic acid functionalized trithiocarbonate or a non-functionalized trithiocarbonate RAFT agent were used to investigate the effect of the end group functionality on

PISA and the dispersion stability. Since PISA is a promising way to generate accurately tunable diblock copolymer compositions and thus a variety of accessible diblock copolymer morphologies, the synthesized P4VP-*b*-PS and P2VP-*b*-PS (for the sake of simplicity PVP-*b*-PS) diblock copolymers were investigated with respect to their film formation behavior. The PVP-*b*-PS diblock copolymers were characterized by gel permeation chromatography (GPC) and proton nuclear magnetic resonance (^{1}H NMR) spectroscopy. Their bulk and film surface morphologies were analyzed *via* transmission electron microscopy (TEM), atomic force microscopy (AFM) and scanning electron microscopy (SEM), respectively. To further investigate the effects on the surface morphology of the diblock copolymer in the thin films, thermal annealing was combined with solvent annealing. Distinct selectivities of different solvents for the individual blocks made it possible to obtain different types of porous surface structures.

Experimental

Materials

Experiments were carried out with Ultrapure water (resistivity >18.2 MΩ cm^{-1}) obtained from a Millipore (Merck, Germany) Direct-Q® UV water purification system. 2,2′-Azobis(2-methyl-propionitrile) (AIBN, 98%, Sigma-Aldrich, Germany, stored at 4 °C), 4-cyano-4-[(dodecylsulfanylthiocarbonyl)-sulfanyl]penta-noic acid (CDTPA, 97%, Sigma-Aldrich, stored at 4 °C), 2-cyano-2-propyl dodecyl trithiocarbonate (CPDTC, 97%, Sigma-Aldrich, stored at 4 °C), chloroform (CHCl$_3$, ≥99.8%, VWR, Germany), *N,N*-dimethylacetamide (DMAc, ≥99.9%, Sigma-Aldrich), methanol (99.9%, Sigma-Aldrich), ethanol (≥99.8%, Sigma-Aldrich), 2-propanol (≥99.5%, Sigma-Aldrich), tetrahydrofuran (THF, 99.8%, Merck), 1,4-dioxane (≥99.5%, Sigma-Aldrich), *N,N*-dimethylformamide (DMF, >99.5%, Merck) and iodine (I$_2$, 99.5%, VWR) were used as received. Styrene (99%, Sigma-Aldrich, contained methyl ether hydroquinone as an inhibitor, stored at 4° C) was freshly percolated through a column of basic aluminum oxide (>98%, Sigma-Aldrich) prior to use to remove the inhibitor. 4-Vinylpyridine (4VP) (97%, Sigma-Aldrich) and 2-vinylpyridine (2VP) (97%, Sigma-Aldrich) were dried over CaH$_2$ (≥95%, Sigma-Aldrich) overnight and distilled under reduced pressure prior to use.

Synthesis of P4VP macroRAFT agent by RAFT bulk polymerization. A typical synthesis of P4VP *via* RAFT bulk polymerization was conducted as follows: CDTPA (43.0 mg, 107 μmol, 1 eq.) and AIBN (0.7 mg, 4 μmol, 0.04 eq.) were dissolved in 4VP (3.15 g, 30 mmol, 281 eq.) ([4VP]/[CDTPA]/[AIBN] = 281/1/0.04). The solution was degassed by purging with nitrogen for 15 min at 0 °C. The bulk polymerization was conducted in a thermoshaker (CellMedia, Germany) at 80 °C and 850 rpm for 4 h and then quenched by ice-cooling and exposure to air. Subsequently, the crude polymer was dissolved in 2-propanol and precipitated in ice-cold *n*-hexane twice. The polymer was dried in vacuum at 40 °C for 24 h and obtained as a light yellow powder. A final 4VP conversion of 69% was calculated

using ^{1}H NMR spectroscopy. The corresponding ^{1}H NMR spectrum is shown in Fig. S1 (ESI).† The apparent number average molecular weight was determined *via* GPC: $\bar{M}_{\text{n,app}}$ = 20 kDa, (theoretical number average molecular weight as calculated by ^{1}H NMR: $\bar{M}_{\text{n,th}}$ = 20 kDa), molecular weight dispersity: Đ = 1.08.

The RAFT polymerization of 4VP with CPDTC was performed similarly. Monomer conversion: 62%, GPC: $\bar{M}_{\text{n,app}}$ = 16 kDa ($\bar{M}_{\text{n,th}}$ = 18 kDa), Đ = 1.08.

Synthesis of P4VP-*b*-PS *via* RAFT dispersion polymerization. A typical procedure was as follows: The P4VP macroRAFT agent/macro-stabilizer (121.4 mg, 6.1 μmol, 1 eq.) was dissolved in methanol/H$_2$O (80/20, v/v) (3.55 mL). Following that, AIBN (0.1 mg, 0.6 μmol, 0.1 eq.) dissolved in methanol (100 μL) was added to the solution. Finally, styrene (609.4 mg, 5.8 mmol, 961 eq.) was added. The total solids content in the formulation amounted to 20 wt%. The solution was degassed by purging with nitrogen for 15 min at 0 °C. The subsequent polymerization was conducted for 24 h at 70 °C and 850 rpm. The polymerization was quenched by ice-cooling and exposure to air. The crude polymer was isolated by removing methanol and H$_2$O under reduced pressure. The polymer was dissolved in THF and poured into an excess of ice-cold *n*-hexane while stirring. This procedure was repeated twice. The polymer was dried in vacuum at 40 °C for 24 h and obtained as a light yellow powder. The corresponding ^{1}H NMR spectrum is shown in Fig. S2.† Monomer conversion: 99%, GPC: $\bar{M}_{\text{n,app}}$ = 104 kDa ($\bar{M}_{\text{n,th}}$ = 119 kDa), Đ = 1.29.

Synthesis of P2VP macroRAFT agent by RAFT bulk polymerization. In order to synthesize the P2VP macroRAFT agent, CDTPA (30.7 mg, 7.6 μmol, 1 eq.) and AIBN (0.5 mg, 3 μmol, 0.04 eq.) were dissolved in 2VP (3.5 g, 3.3 mmol, 438 eq.) ([2VP]/[CDTPA]/[AIBN] = 438/1/0.04). The experimental work-up was the same as described above for the synthesis of the P4VP macroRAFT agent. The corresponding ^{1}H NMR spectrum is shown in Fig. S1.† Monomer conversion: 53%, GPC: $\bar{M}_{\text{n,app}}$ = 21 kDa ($\bar{M}_{\text{n,th}}$ = 25 kDa), Đ = 1.26. The RAFT polymerization of 2VP with CPDTC was performed accordingly. Monomer conversion: 53%, GPC: $\bar{M}_{\text{n,app}}$ = 21 kDa ($\bar{M}_{\text{n,th}}$ = 25 kDa), Đ = 1.25.

Synthesis of P2VP-*b*-PS *via* RAFT dispersion polymerization. For a typical synthesis of P2VP-*b*-PS, the P2VP macroRAFT agent (469 mg, 2.4 μmol, 1 eq.) was dissolved in methanol/ H$_2$O (80/20, v/v) (11.82 mL). AIBN (0.4 mg, 2.4 μmol, 0.1 eq.) in methanol (100 μL) was added to the solution, followed by the addition of styrene (1.9 g, 1.9 mmol, 775 eq.). The subsequent experimental procedure was the same as for the synthesis of P4VP-*b*-PS. The corresponding ^{1}H NMR spectrum is shown in Fig. S2.† Monomer conversion: 91%, GPC: $\bar{M}_{\text{n,app}}$ = 109 kDa ($\bar{M}_{\text{n,th}}$ = 93 kDa), Đ = 1.06.

Characterization

^{1}H NMR spectroscopy. ^{1}H NMR spectroscopy experiments were performed using a Bruker AV500 spectrometer. ^{1}H NMR spectra were recorded applying a 10 ms 90° pulse at a sample temperature of 298 K. 16 scans were recorded with a relaxation delay of 3 s. Sample concentrations were 20 g L^{-1} in THF-d$_8$ or

CDCl$_3$, respectively. The NMR spectra were analyzed with the software MestReNova 10.0.

The conversion of 4VP was determined in CDCl$_3$ by ^{1}H NMR from the integral ratio of the aromatic P4VP signal at 8.48–8.09 ppm and the monomer signal at 8.55 ppm. The conversion of styrene in the dispersion polymerization, determined in THF-d$_8$, was calculated from the decrease of the integral of the monomer peaks. Therefore a reference sample was taken prior to and at the end of the polymerization. The aromatic P4VP signal at 8.48–8.09 ppm was used as a reference. The conversion in P2VP and P2VP-b-PS experiments was estimated analogously.

Gel permeation chromatography (GPC). The molecular weights of the PVP homopolymers and PVP-b-PS diblock copolymers were obtained using a DMAc GPC at 50 °C with the addition of lithium chloride (0.1 M). A Waters 717 plus instrument equipped with PSS GRAM columns [GRAM pre-column (dimension 8–50 mm) and two GRAM columns of different porosity (3000 Å and 1000 Å)] with dimensions of 8 × 300 mm and a particle size of 10 μm was employed. The samples were measured at a flow rate of 1 mL min^{-1} using a VWR-Hitachi 2130 pump and a Shodex RI-101 refractive index detector. GPC was calibrated with narrow PS standards and data were analyzed using PSS WinGPC UniChrom software.

Atomic force microscopy (AFM). AFM images were obtained on a Bruker MultiMode 8 atomic force microscope (BrukerNano, Germany) operating in PeakForce QNM® (Quantitative Nanomechanical Mapping) mode at room temperature using SCANASYST-AIR cantilevers (spring constant 0.4 N m^{-1}, silicon tip of 2 nm radius). The images were evaluated with the Nanoscope 9.2 Software (BrukerNano). Thin films for AFM measurements were prepared as follows: Silicon (Si) wafer substrates sized 1 cm × 1 cm were rinsed with CH$_2$Cl$_2$, further cleaned with a mixture of H$_2$O, H$_2$O$_2$ and NH$_4$OH (60/20/20, v/v/v), rinsed with H$_2$O and directly before use treated with H$_2$/O$_2$ plasma. Thin films with a thickness of about 150 nm were generated by spin-coating 2 wt% diblock copolymer solutions in CHCl$_3$, a rather non-selective solvent for both blocks, onto the Si wafer substrates. A spin-coater G3P-8 (Specialty Coating Systems, USA) was operated at 3000 rpm for 60 s. The samples were stored in a desiccator at room temperature.

Additional, thermal annealing of the samples was conducted at a temperature $T_{annealing}$ = 180 °C in vacuum for 15 h. For the topography microphase reconstruction two different methods were followed: (a) the spin-coated samples were exposed for 10 min in 1,4-dioxane vapor at room temperature followed by dip-coating in ethanol for 5 min and drying under vacuum at room temperature for 10 h and (b) the samples were dip-coated in dimethylformamide for 3 s, exposed to air for 5 min and subsequently immersed in water for 3 h followed by air exposure for 10 h.

Scanning electron microscopy (SEM). SEM images were taken with a scanning electron microscope Merlin (Carl ZEISS, Germany) at accelerating voltages of 0.7–2.0 kV of 150 nm thick P4VP-b-PS and P2VP-b-PS films on Si wafer substrates

prepared for the AFM measurements. To obtain a better contrast between the microphases, P4VP and P2VP were selectively stained in I$_2$-vapor for 15 min, following a process previously published.[59] These samples were not sputter coated and investigated at low acceleration voltage with the use of an energy selective backscattered (EsB) electron detector or a secondary electron (SE) detector. For the estimation of the surface pores the samples were sputtered with 0.5 nm platinum and examined using an SE detector.

Transmission electron microscopy (TEM). The morphology of the diblock copolymers was investigated *via* TEM using a Tecnai G2 F20 electron microscope (Thermo Fisher Scientific, The Netherlands), operating at an accelerating voltage of 120 kV in bright field mode. Polymer films were cast from solutions in CHCl$_3$ and slowly dried in the presence of solvent vapor in a desiccator for 2 weeks. The P4VP-b-PS films were further annealed thermally, stepwise, up to 160 °C in vacuum. Analogously, the P2VP-b-PS films were annealed thermally, stepwise, up to 125 °C in vacuum. Ultrathin sections of approximately 50 nm were cut with a Leica Ultramicrotome EM UCT (Leica Microsystems, Germany) equipped with a diamond knife (Diatome AG, Switzerland). P4VP and P2VP were selectively stained in I$_2$-vapor for 2 h.

Results and discussion

For RAFT-mediated dispersion polymerization, the choice of the macroRAFT agent and solvent are crucial in order to polymerize a certain monomer. The macroRAFT agent acts as a steric stabilizer and plays a key role in keeping the system stable and obtaining monodisperse block copolymers. In the present work, RAFT dispersion polymerizations of styrene were conducted using PVP macroRAFT agents. The PVP-b-PS diblock copolymers were prepared *via* a two-step RAFT polymerization (Fig. 1). Either CDTPA or CPTTC-terminated PVP was synthesized first *via* bulk polymerization and then used as the macroRAFT agent in the dispersion polymerization of styrene, forming the desired PVP$_k$-PS$_m$ diblock copolymers with k and m being the mean degrees of polymerization (DPs) of PVP and PS, respectively. An 80 : 20 methanol/water mixture was selected as the continuous phase for these RAFT dispersion polymerization formulations.

RAFT bulk polymerization and surfactant-free RAFT dispersion polymerization

The RAFT bulk polymerizations were stopped at monomer conversions <70% to maintain a high fidelity of the trithiocarbonate functionality and avoid the occurrence of an excess of termination products from coupling reactions.[60,61] Moreover, early termination facilitates further processing by prevention of excessive viscosity of the bulk sample. The two homopolymers P4VP and P2VP vary in molecular weight as well as the RAFT end-group. One aim of this study was to identify suitable RAFT agents for the subsequent PISA with styrene through RAFT-mediated dispersion polymerization. Table 1 summar-
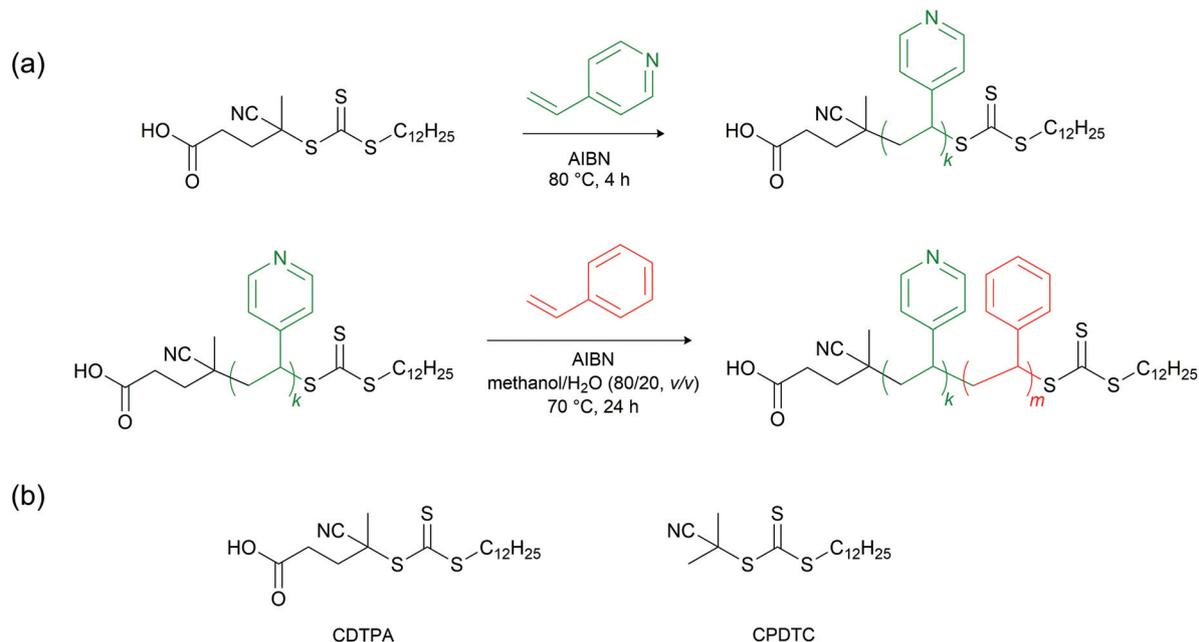
Fig. 1 (a) Exemplary synthetic route to P4VP$_k$-PS$_m$ diblock copolymers using the CDTPA RAFT agent. Synthesis of the P4VP-CDTPA macroRAFT agent by RAFT bulk polymerization followed by the synthesis of P4VP$_k$-PS$_m$ *via* surfactant-free RAFT dispersion polymerization in methanol/water (80/20, v/v). The synthesis of P2VP$_k$-PS$_m$ was conducted accordingly with a P2VP-CDTPA macroRAFT precursor; (b) chemical structure of the two trithiocarbonate RAFT agents used in this study.

Table 1 Summary of the synthesized P2VP and P4VP homopolymers with assignment of their end group according to the RAFT agent used

Homopolymer[a]	$\bar{M}_{\text{n,app}}$[b] [kDa]	$\bar{M}_{\text{w,app}}$[b] [kDa]	Conv. [%]	$\bar{M}_{\text{n,th}}$[c] [kDa]	Đ	RAFT agent
P4VP$_{186}$	20	22	69	20	1.08	CDTPA
P4VP$_{168}$	16	18	62	18	1.08	CPDTC
P2VP$_{234}$	21	27	53	25	1.26	CDTPA
P2VP$_{234}$	21	26	53	25	1.24	CDTPA
P2VP$_{234}$	21	26	53	25	1.25	CPDTC
P2VP$_{215}$	19	23	52	23	1.20	CDTPA
P2VP$_{186}$	20	25	46	20	1.27	CDTPA

[a] Superscripts denote the mean DPs as determined by ^{1}H NMR spectroscopy. [b] The apparent molecular weights $\bar{M}_{\text{n,app}}$ and $\bar{M}_{\text{w,app}}$ were determined by DMAc GPC calibrated with PS standards. [c] $\bar{M}_{\text{n,th}}$ was calculated as follows: $\bar{M}_{\text{n,th}}$ = [monomer]/[RAFT] × M_{monomer} × monomer conversion + M_{RAFT}. M: molecular weight.

izes the PVP homopolymers and their respective analytical data.

For the following RAFT dispersion polymerization (Fig. 1), the P4VP macroRAFT agent was dissolved in an 80 : 20 methanol/water mixture. The comparison of the Hansen solubility parameters shows that the solubility of styrene is higher in methanol than in water (Table S1†). However, the styrene solubility in the chosen reaction medium is kept sufficiently high to justify a true dispersion polymerization mechanism, which initially proceeds homogeneously until a critical PS block length is exceeded. More importantly, water as a co-solvent significantly worsens the solvency for the growing polystyrene chains.[41] This lowers the critical mean DP required for micellar nucleation. The initial (slow) homogeneous polymerization more rapidly turns into a faster dispersion polymerization, in

which the polymerization occurs within the monomer-swollen micelles.[40,42]

Characterization of the PVP-*b*-PS diblock copolymers *via* ^{1}H NMR and GPC

P4VP/P2VP served as macroRAFT agent and macro-stabilizer in the RAFT dispersion polymerization of styrene in methanol/water (80/20, v/v) and AIBN as the initiator of the reaction. Styrene, as well as the P4VP macroRAFT agent and AIBN are soluble in the 80 : 20 methanol/water mixture. Thus, the polymerization, or more precisely the chain extension of PVP with styrene, starts homogeneously until a critical PS block length is exceeded and the PVP-*b*-PS chains start to self-assemble into micelles. In the dispersion polymerization of styrene, a quantitative monomer conversion (93–99%) was reached, as indicated by ^{1}H NMR. The apparent number-average molecular

weights ($\bar{M}_{n,app}$) of the PVP-b-PS diblock copolymers were obtained *via* GPC. The GPC curves of the P4VP-b-PS diblock copolymers reveal that the curves corresponding to the diblock copolymers significantly shift towards higher molecular weights compared to the respective macroRAFT agents (Fig. 2). Additionally, the GPC traces show dispersities of $Đ = 1.14–1.29$, which indicate well-controlled RAFT dispersion polymerizations. This is further evidenced by the observation of hardly any homopolymer impurities in the GPC traces. The PS fraction in the P4VP-b-PS diblock copolymers is approximately 79–83% by weight as obtained by ^{1}H NMR. The respective diblock copolymers as well as ^{1}H NMR and GPC data are depicted in Table 2.

The RAFT agent, which contains a dodecyl end-group on the ω-terminal-end of the polymer chain and a carboxylic acid group as well as a cyano group on the α-terminal end, is slightly more hydrophilic compared to the RAFT agent with similar chain length but only a cyano-group on the α-terminal

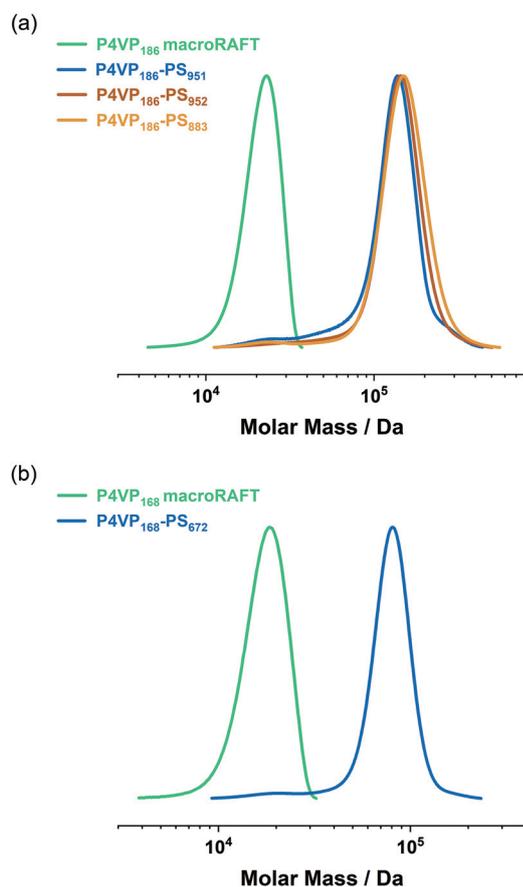end. To quantify this statement, the *n*-octanol–water partition coefficient log P, a measure of the hydrophilicity of a chemical compound, is determined. It is negative for polar substances and positive for non-polar substances. The values obtained were calculated log P (C log P) values using ChemDraw 13.0 (PerkinElmer, United States of America). The C log P for CDTPA was calculated as 6.76, while the C log P for CPDTC was determined to be 7.64. Hence, CDTPA is slightly more hydrophilic than CPDTC. Surprisingly, exchanging the carboxylic acid on the α-terminal end with a less hydrophilic residue does not significantly influence PISA. Hence, the RAFT dispersion polymerizations of styrene with CDTPA- or CPDTC-terminated macroRAFT agents exhibit similar monomer conversions. The difference between the monomers 4VP and 2VP, especially regarding the molar masses and dispersities achieved in the homopolymerizations, is probably more decisive than the choice of RAFT agent regarding the two trithiocarbonates to be compared. If 4VP is replaced by 2VP, an isomer that differs only in the position of the nitrogen atom, the homopolymerization results in approximately 10% lower monomer conversions. From GPC traces (Fig. 3), it becomes evident that the results for P2VP-b-PS are similar compared to the P4VP-b-PS experiments. However, for P2VP$_{234}$-PS$_{663}$ and P2VP$_{234}$-PS$_{739}$ there are a residual amount of P2VP$_{234}$ macroRAFT agent in the diblock copolymer GPC traces. This homopolymer impurity, which accounts for approximately 5% of the total polymer, can probably be attributed to unreacted macroRAFT agent chains. For other P2VP$_{215}$-PS$_{672}$ and P2VP$_{215}$-PS$_{595}$ diblock copolymers, hardly any macroRAFT residues were visible in the GPC traces. When evaluating the chromatograms quantitatively, however, it becomes apparent that the P2VP-b-PS diblock copolymer peaks on their own show very low dispersities ($Đ = 1.06–1.11$) and, due to styrene conversions of almost 90%, as indicated by ^{1}H NMR, in most cases, also exhibit high molecular weights of over 100 kDa (Table 2).

To summarize, the chosen RAFT aqueous-alcoholic dispersion polymerization method is suitable for producing high molecular weight diblock copolymers under simple reaction conditions in acceptable reaction times. This synthetic route, which does not require surfactants or other additives, not only demonstrates the preparation of PVP-b-PS diblock copolymers with molecular weights above 130 kDa ($\bar{M}_{n,app}$), but also enables the synthesis of relatively narrow molecular weight distributed polymers with monomer conversions of 86–99%. Hence, this RAFT-mediated PISA approach enables the synthesis of diblock copolymers in molecular weight ranges and qualities that are normally only obtained by anionic polymerization methods.[62–64]

Morphological investigation of PVP-b-PS diblock copolymers

Transmission electron microscopy (TEM). To investigate the bulk morphology, transmission electron microscopy (TEM) measurements were performed on the PVP-b-PS diblock copolymer films, obtained from solution casting from CHCl$_3$. The solvent was slowly evaporated in the presence of solvent vapor and the films were further annealed above the glass transition

Fig. 2 GPC curves recorded for (a) a P4VP$_{186}$ macroRAFT agent and the corresponding P4VP$_{186}$-PS$_m$ diblock copolymers. The shift of the diblock copolymer curves towards higher molecular weights indicates the successful RAFT dispersion polymerization, (b) a P4VP$_{168}$ macroRAFT agent and the corresponding P4VP$_{168}$-PS$_m$ diblock copolymer. A well-controlled RAFT dispersion polymerization is indicated by low dispersities ($Đ = 1.14–1.29$) of the final P4VP-b-PS diblock copolymers.

Table 2 Summary of the synthesized PVP-b-PS diblock copolymers

PVP-PS composition[a]	$\bar{M}_{n,app}$[b] [kDa]	$\bar{M}_{w,app}$[b] [kDa]	Conv. [%]	$\bar{M}_{n,th}$[c] [kDa]	Đ	f_{PVP} [wt%]	RAFT agent
P4VP186-PS951	104	135	99	119	1.29	17	CDTPA
P4VP186-PS952	122	147	99	120	1.20	17	CDTPA
P4VP168-PS672	70	79	99	88	1.14	21	CPDTC
P4VP186-PS883	125	155	93	112	1.24	19	CDTPA
P2VP234-PS768	137	152	87	105	1.11	24	CDTPA
P2VP234-PS663	130	144	87	94	1.11	27	CDTPA
P2VP234-PS739	136	150	87	102	1.11	24	CDTPA
P2VP234-PS566	119	131	86	84	1.10	29	CPDTC
P2VP215-PS672	109	116	91	93	1.06	24	CDTPA
P2VP215-PS595	92	97	86	85	1.06	27	CDTPA

[a] Superscripts denote the mean DPs as determined by ^{1}H NMR spectroscopy. [b] Determined by DMAc GPC calibrated with PS standards. For P2VP$_k$-PS$_m$, the GPC curve peaks were analysed separately and assigned as precursor and diblock copolymer peak. [c] $\bar{M}_{n,th}$ was calculated as follows: $\bar{M}_{n,th}$ = [monomer]/[macroRAFT] × $M_{monomer}$ × monomer conversion + $M_{macroRAFT}$.
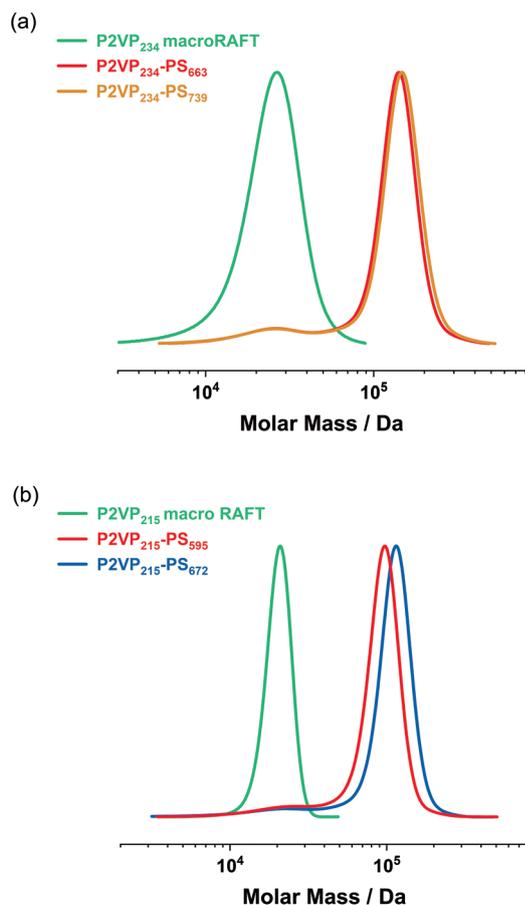

Fig. 3 GPC curves recorded for (a) a P2VP234 macroRAFT agent and the corresponding P2VP234-PS$_m$ diblock copolymers; (b) a P2VP215 macroRAFT agent and the corresponding P2VP215-PS$_m$ diblock copolymers.

temperature of both blocks. Ultrathin sections of approximately 50 nm were cut and P4VP and P2VP microphases were selectively stained in I$_2$-vapor for 2 h.

Fig. 4 shows TEM images of the P4VP-b-PS and P2VP-b-PS diblock copolymers. For P4VP186-PS951 with a P4VP weight frac-

tion of 17% P4VP and an $\bar{M}_{n,th}$ of 119 kDa a spherical morphology of P4VP spheres in a continuous PS matrix was identified. The sample P4VP168-PS672, with an increased P4VP weight fraction of 21% and a lower $\bar{M}_{n,th}$ of 88 kDa, shows the coexistence of hexagonally arranged cylinders and spheres (Fig. 4c and d). Areas with perpendicularly and parallel cut cylinders are observed elongated and oriented in a mutual direction. Considering the different sample positions and sections, spherical areas were identified as directly adjacent to the cylindrical areas. Due to their size and arrangement, the perpendicularly cut cylinders could be easily distinguished from the spheres, which are smaller and do not show a hexagonal arrangement. For a P2VP215-PS672 bulk film, with a P2VP weight fraction of 24% and a total $\bar{M}_{n,th}$ of 93 kDa, a cylindrical morphology with hexagonally arranged P2VP cylinders was observed, with the cylinders found parallel and perpendicularly oriented to the plane (Fig. 4e and f). The results show, that the homopolymer impurities do not alter the morphologies of the PVP-b-PS diblock copolymers.

Atomic force microscopy (AFM) and scanning electron microscopy (SEM). Thin block copolymer films exhibit ordered periodic microdomains such as spheres, cylinders and lamellae. The size, shape and orientation of the microdomains can be controlled by chain length, chemical composition, weight fraction of the blocks and external factors such as solvent and temperature.[52] The surface morphology of thin PVP-b-PS films with different molecular weights and weight fractions of the diblock copolymers was examined via atomic force microscopy (AFM) and scanning electron microscopy (SEM). For AFM and SEM measurements, diblock copolymer thin films were prepared by spin-coating of 2 wt% PVP-b-PS in CHCl$_3$ solutions onto silicon-wafer substrates. CHCl$_3$ was chosen because of its low boiling point and lack of selectivity with respect to one of the two blocks. Spin-coating was followed by thermal and solvent annealing to optimize the microstructures of the diblock copolymers. Thermal annealing was conducted at $T_{annealing}$ = 180 °C in vacuum, above the glass transition temperature (T_g) of both blocks. In order to increase the chain mobility, thermal annealing was combined with solvent annealing. The chosen solvents are known to confer greater
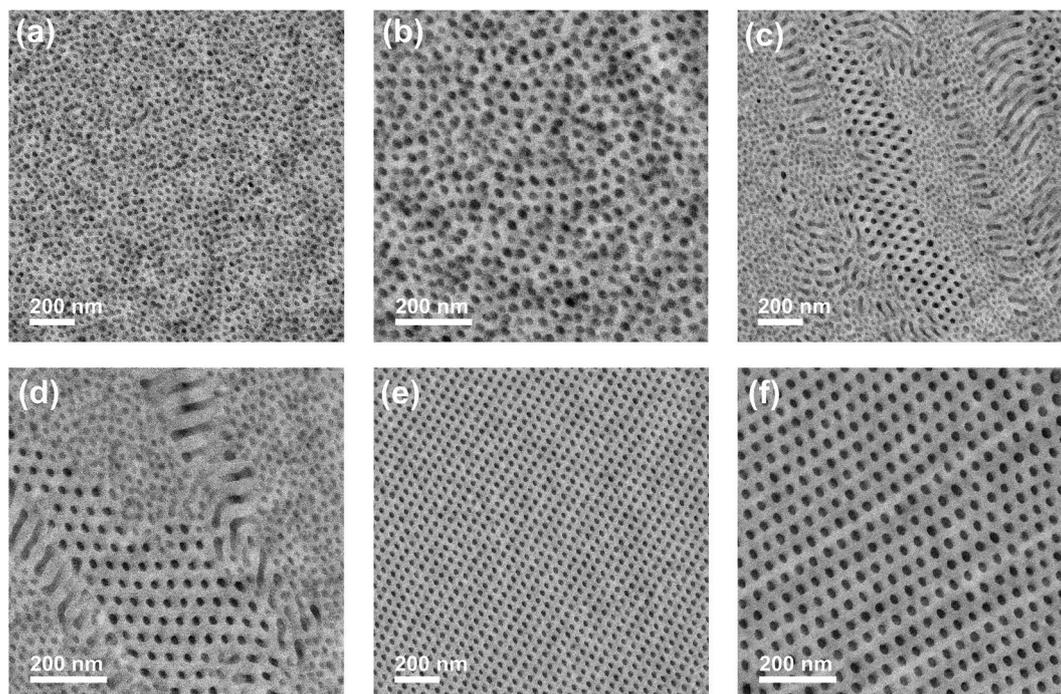
Fig. 4 TEM images of the PVP-*b*-PS bulk films. The bright areas correspond to the polystyrene microphase in the TEM images. (a and b) TEM image of a $P4VP_{186}$-PS_{951} bulk structure; (c and d) TEM image of a $P4VP_{168}$-PS_{672} bulk structure; (e and f) TEM image of a $P2VP_{215}$-PS_{672} bulk structure.

chain motion within thin films and interact selectively with the two blocks.[65] On a microscopic level, the microdomains of the diblock copolymer are swollen and dried during solvent annealing. A combination of 10 min 1,4-dioxane vapor annealing followed by 5 min dip-coating in ethanol was chosen. 1,4-Dioxane, which is a selective solvent for the PS block, mobilizes the PS matrix while ethanol, selective for PVP, softens and swells the PVP phase leading to a nanoporous film with the minor PVP phase located in the pore as well as on the surface of the film. This process is well described in the literature.[52,66,67] For example, Park *et al.* discovered that it did not affect either the order or orientation of the P4VP microdomains in a PS matrix.[68] Of particular interest are cylindrical oriented microdomains {perpendicular to the surface} because degradation and removal of the minor component transforms these structures into nanoporous templates.[69,70] However, this process is irreversible as it alters the chemical composition. In order to overcome this disadvantage, Park *et al.* developed a fully reversible surface reconstruction process for the preparation of nanoporous films without eliminating the minor polymer component.[68]

Fig. 5 shows six AFM QNM height images of pristine and annealed spin-coated diblock copolymer films. Pristine spin-coated films of the diblock copolymers show a relatively flat but microphase-separated surface, with the respective morphology depending on both layer thickness and copolymer composition. However, all of the pristine sample films show not perfectly delimited microstructures. The PS phase (Fig. 5a, d and g) appears bright and the PVP phase dark. Upon

Fig. 5 Surface topography studies *via* QNM AFM height images (1 μm × 1 μm) of spin-coated thin films of (a) $P4VP_{186}$-PS_{951} pristine, (b) $P4VP_{186}$-PS_{951} thermally annealed at 180 °C followed by 10 min 1,4-dioxane vapor annealing, (c) $P4VP_{186}$-PS_{951} after thermal annealing at 180 °C followed by 10 min 1,4-dioxane vapor annealing and subsequent dip-coating in ethanol for 5 min; (d) $P4VP_{168}$-PS_{672} pristine; (e) $P4VP_{168}$-PS_{672} thermally and 1,4-dioxane vapor annealed; (f) $P4VP_{168}$-PS_{672} dip-coated in ethanol; (g) $P2VP_{215}$-PS_{672} pristine; (h) $P2VP_{215}$-PS_{672} thermally and 1,4-dioxane vapor annealed; (i) $P2VP_{215}$-PS_{672} dip-coated in ethanol. The PS phase appears bright.

thermal annealing, the chain mobility is increased and the surface is flattened (Fig. S3 and S4†). Additional AFM images were taken after the two-step solvent annealing process. The AFM height image of a thin spin-coated P4VP$_{186}$-PS$_{951}$ film, with a P4VP weight fraction of 17%, shows distinct spherical P4VP microdomains in a continuous PS matrix after 1,4-dioxane vapor annealing, which enhanced the microphase separation and diminished defects in the microstructure of the diblock copolymer. The PS phase (Fig. 5b, e and h) appears dark and PVP bright, due to swelling of the phase. Subsequent dip-coating in ethanol generated a porous spherical microstructure due to the collapse of the P4VP microphase. The PS phase (Fig. 5c, f and i) appears bright, the pores appear dark and the PVP phase, which is collapsed, appears as a bright ring surrounding the pores. For a chosen diblock copolymer, with a higher P4VP weight fraction of 21% (P4VP$_{168}$-PS$_{672}$) and a lower $\bar{M}_{n,th}$ of 88 kDa, a cylindrical microstructure was found in AFM height images after solvent annealing. Dip-coating in ethanol produced a porous cylindrical surface microstructure. Regarding P2VP-b-PS, a diblock copolymer with a P2VP weight fraction of 24% and a total $\bar{M}_{n,th}$ of 93 kDa (P2VP$_{215}$-PS$_{672}$),

shows a porous cylindrical microstructure after the two-step solvent annealing process. Fig. 6 shows SEM images of the PVP-b-PS diblock copolymer thin films. The images were taken of the pristine films, after therma l annealing followed by 1,4-dioxane vapor annealing and after final dip-coating in ethanol. The PS phase (Fig. 6) appears dark and the PVP phase bright. The brighter rings surrounding the pores (Fig. 6c, f and i) can be assigned to the electron-rich iodine, which selectively stained the PVP phase.[71] Due to its high atomic number (53), iodine leads to strong backscattering of electrons.[59] Although SEM and AFM produce similar representations of the thin film surface structure, SEM enabled to capture a large area view of the surface structure at once, while AFM only allowed to view 1 μm × 1 μm areas. Hence, SEM images confirmed that large-scale porous surface structures were created by the surface reconstruction annealing process. In order to further investigate the impact of solvent annealing, to control the alignment of the thin film topography, as well as to obtain a modified isoporous topographical structure, a further annealing technique was developed. Based on results from the structure formation of isoporous membranes by non-solvent induced phase separ-
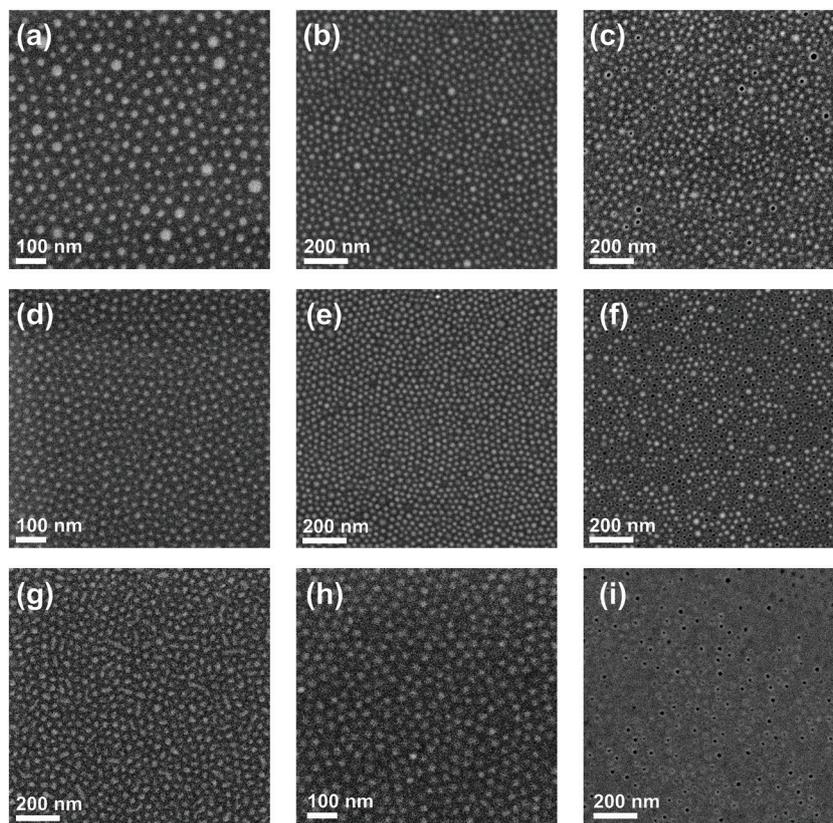

Fig. 6 SEM images (EsB detector) of spin-coated thin films of a 2 wt% PVP-b-PS CHCl$_3$ solution prior to and after thermal combined with solvent annealing. (a) P4VP$_{186}$-PS$_{951}$ pristine spin-coated thin film, (b) P4VP$_{186}$-PS$_{951}$ thermally annealed at 180 °C followed by 10 min 1,4-dioxane vapor annealing, (c) P4VP$_{186}$-PS$_{951}$ after thermal annealing at 180 °C followed by 10 min 1,4-dioxane vapor annealing and subsequent dip-coating in ethanol for 5 min; (d) P4VP$_{168}$-PS$_{672}$ pristine; (e) P4VP$_{168}$-PS$_{672}$ thermally and 1,4-dioxane vapor annealed; (f) P4VP$_{168}$-PS$_{672}$ dip-coated in ethanol; (g) P2VP$_{215}$-PS$_{672}$ pristine; (h) P2VP$_{215}$-PS$_{672}$ thermally and 1,4-dioxane vapor annealed; (i) P2VP$_{215}$-PS$_{672}$ dip-coated in ethanol. PS appears as dark grey, P4VP as light grey and the pores appear black. In (c), (f) and (i) the brighter rings around the pores can be assigned to the P4VP phase stained by the electron rich iodine.

ation (NIPS),[72,73] a process partially imitating NIPS was followed. To investigate the effects of solvent exchange on the topography, the thin film on the Si-wafer was first dip-coated in a solvent {selective for one block} and then immersed into a non-solvent for both blocks. More precisely, the thermally annealed diblock copolymer thin film was dip-coated in DMF for 3 seconds, dried for 5 minutes in the presence of air and finally immersed into a water bath for 3 hours. Dry DMF was found to completely dissolve the thin film within 3 s. Therefore, water was added to DMF in amounts of 5–12 vol%. A DMF/water mixture of 92/8 v/v led to the best results regarding pore formation and was used for further experiments. Dip-coating in DMF, which is a good solvent for both blocks of the diblock copolymer but a selective solvent for the PVP block, {according to the solubility parameters of the solvents and blocks[74,75]} leads to highly swollen, soft PVP domains. Upon immersion in water, a non-solvent for both blocks, the initial microstructure is conserved and the PVP chains collapse with their domains forming open pores.[72] According to the previous assumption, the AFM height image of a DMF/water annealed P4VP$_{186}$-PS$_{951}$ film shows an isoporous spherical microstructure with more uniformly arranged pores (Fig. 7) compared to a 1,4 dioxane/ethanol annealed P4VP$_{186}$-PS$_{951}$ film (Fig. 5 and 6). The diblock copolymer (Fig. 7) appears grey (SEM) or bright (AFM) while the pores appear dark.

In order to correlate the different porous structures obtained by the two different solvent annealing techniques

quantitatively, the pore sizes were determined from SEM images of samples sputter coated with 0.5 nm platinum using the software Imagic IMS (Imagic Bildverarbeitung AG, Switzerland). Measurements yielded mean pore diameters for a DMF/water annealed P4VP$_{186}$-PS$_{951}$ film and a 1,4 dioxane/ethanol annealed P4VP$_{186}$-PS$_{951}$ film to be 17.6 nm ± 4.0 nm and 11.7 nm ± 5.5 nm, respectively. Hence, the mean pore diameter of the DMF/water annealed P4VP$_{186}$-PS$_{951}$ film was 1.5 times larger than the mean pore diameter determined for the 1,4 dioxane/ethanol annealed P4VP$_{186}$-PS$_{951}$ film. Furthermore, the DMF/water annealed P4VP$_{186}$-PS$_{951}$ film shows a lower standard deviation of the mean pore diameter and a higher order in terms of pore diameter distribution. The median pore diameter is 17.7 nm for the DMF/water annealed sample and 10.5 nm for the 1,4-dioxane/ethanol annealed sample, which for the latter shows a significantly larger deviation from the mean pore diameter and thus a more inhomogeneous pore size distribution. A similar pore diameter deviation was found for P2VP$_{215}$-PS$_{672}$ when comparing the two annealing processes. The mean pore diameter determined for the P2VP$_{215}$-PS$_{672}$ thin film after DMF/water annealing (Fig. 7) was 21.3 nm ± 3.5 nm (median pore diameter 21.8 nm) and 15.4 nm ± 6 nm (median pore diameter 14.0 nm) for the 1,4-dioxane/ethanol annealed film (Fig. 6). Thus, DMF/water annealing led to a 1.4 times larger mean pore diameter and a narrower pore size distribution.

Regarding the self-assembly properties, the PVP-b-PS diblock copolymers of this work are well comparable with the self-assembly properties of PS-b-PVP diblock copolymers obtained via anionic polymerization, previously mentioned in literature. Gallei et al. and Jung et al. investigated the structure formation of isoporous membranes of PS-b-P4VP and PS-b-P2VP, respectively.[76,77] The examined diblock copolymers had similar molecular weights and block compositions in the region wherein PVP is expected to form spherical or cylindrical domains in bulk.
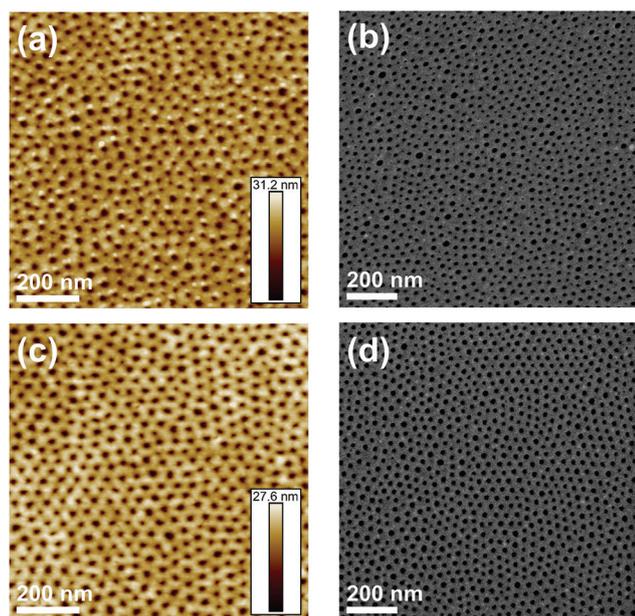

Fig. 7 AFM and SEM studies of spin-coated thin films of a 2 wt% PVP-b-PS CHCl$_3$ solution. The films were dip-coated in DMF for 3 s, exposed to air for 5 min and immersed in water for 3 h. Surface topography via QNM AFM height images (1 µm × 1 µm) and SEM images (SE detector) of the isoporous thin films. The diblock copolymer appears grey (SEM) or bright (AFM) while the pores appear dark. (a) AFM image and (b) SEM image of a DMF/water annealed P4VP$_{186}$-PS$_{951}$ thin film; (c) AFM image and (d) SEM image of a DMF/water annealed P2VP$_{215}$-PS$_{672}$ thin film.

Conclusions

In this work, the synthesis of high molecular weight P4VP-b-PS and P2VP-b-PS diblock copolymers was performed in a two-step process of a RAFT bulk polymerization followed by a surfactant-free RAFT dispersion polymerization. A series of P4VP and P2VP homopolymers with dispersities ranging from 1.08–1.27 were prepared via RAFT bulk polymerization at 80 °C using two different trithiocarbonate RAFT agents. The choice of RAFT agent did not show significant effects on monomer conversion or dispersity.

A PVP macroRAFT agent was chain extended via RAFT aqueous-alcoholic dispersion polymerization of styrene at 70 °C and 20% w/w solids content, reaching quantitative conversion within 24 h as indicated by ^{1}H NMR. A series of PVP-b-PS diblock copolymers was prepared with high $\bar{M}_n$ between 70 and 137 kDa and low dispersities as evaluated by ^{1}H NMR and GPC. The proposed particle formation mechanism is the

polymerization-induced self-assembly (PISA), which involves the *in situ* formation of micellar objects after initial chain growth in the aqueous-alcoholic phase. In the bulk state the block copolymers microphase separate into regularly ordered cylindrical or spherical morphologies, as revealed by TEM.

Spin-coated PVP-*b*-PS diblock copolymer films with weight fractions of the minority PVP block ranging from 17–24% were converted to porous structures by a selective alignment and swelling strategy and investigated *via* AFM and SEM.

A comparison of two annealing procedures aiming to obtain isoporous thin films was performed. The first approach combined thermal annealing with 1,4-dioxane vapor annealing, followed by dip-coating in ethanol. The second technique comprised thermal annealing, followed by dip-coating in DMF and immersion into water. Both procedures led to porous structures, but with structural differences. DMF/water annealed $P4VP_{186}$-PS_{951} and $P2VP_{215}$-PS_{672} films showed an isoporous spherical surface microstructure with more uniformly arranged pores compared to the corresponding films annealed in 1,4 dioxane/ethanol. Moreover, measurements revealed that the mean pore diameter of the filmes annealed in DMF/water were approximately 1.5 times larger with a lower standard deviation than the mean pore diameter of the corresponding films annealed in 1,4 dioxane/ethanol. The modified porous topographical structures were obtained by distinct selectivities of the different solvents for the individual blocks. Hence, the study showed a variable pore alignment and pore swelling by solvent annealing with different solvent combinations. When annealing with DMF/water, isoporous thin films could be prepared when using either P2VP-*b*-PS or P4VP-*b*-PS diblock copolymers.

Conflicts of interest

There are no conflicts to declare.

Author contributions

K.N. and P.G.: conceptualization; K.N. and P.G.: methodology, investigation, data curation, formal analysis, validation; P.G. and V.A.: supervision. V.A.: resources, K.N. and P.G.: writing – original draft, K.N., P.G. and V. A.: writing – review & editing.

Acknowledgements

Notes and references

1   E. Rizzardo and D. H. Solomon, *Aust. J. Chem.*, 2012, **65**, 945–969.
2   A. D. Jenkins, R. G. Jones and G. Moad, *Pure Appl. Chem.*, 2009, **82**, 483–491.
3   K. Matyjaszewski, B. S. Sumerlin and N. V. Tsarevsky, *ACS Publ.*, 2012, **1100**, 1–13.
4   D. Roy, J. N. Cambre and B. S. Sumerlin, *Chem. Commun.*, 2008, 2477–2479.
5   C. L. McCormick and A. B. Lowe, *Acc. Chem. Res.*, 2004, **37**, 312–325.
6   T. G. Ribelli, D. Konkolewicz, S. Bernhard and K. Matyjaszewski, *J. Am. Chem. Soc.*, 2014, **136**, 13303–13312.
7   J.-T. Sun, C.-Y. Hong and C.-Y. Pan, *Polym. Chem.*, 2013, **4**, 873–881.
8   V. Delplace, E. Guégain, S. Harrisson, D. Gigmes, Y. Guillaneuf and J. Nicolas, *Chem. Commun.*, 2015, **51**, 12847–12850.
9   M. R. Hill, R. N. Carmean and B. S. Sumerlin, *Macromolecules*, 2015, **48**, 5459–5469.
10 W. D. Harkins, *J. Am. Chem. Soc.*, 1947, **69**, 1428–1444.
11 G. Lichti, R. G. Gilbert and D. H. Napper, *J. Polym. Sci., Polym. Chem. Ed.*, 1983, **21**, 269–291.
12 W. D. Harkins, *J. Polym. Sci.*, 1950, **5**, 217–251.
13 C. Barner-Kowollik, *Handbook of RAFT Polymerization*, John Wiley & Sons, Weinheim, 2008.
14 R. G. Gilbert, *Emulsion polymerization: a mechanistic approach*, Academic Press, London, 1995.
15 J. Goodwin, J. Hearn, C. Ho and R. Ottewill, *Colloid Polym. Sci.*, 1974, **252**, 464–471.
16 F. Lauterbach and V. Abetz, *Soft Matter*, 2020, **16**, 2321–2331.
17 M. Semsarilar and S. Perrier, *Nat. Chem.*, 2010, **2**, 811–820.
18 K. Nieswandt, P. Georgopanos, C. Abetz, V. Filiz and V. Abetz, *Materials*, 2019, **12**, 3145.
19 J. Rieger, C. Grazon, B. Charleux, D. Alaimo and C. Jérôme, *J. Polym. Sci., Part A: Polym. Chem.*, 2009, **47**, 2373–2390.
20 Y. Li and S. P. Armes, *Angew. Chem.*, 2010, **122**, 4136–4140.
21 J. Rieger, *Macromol. Rapid Commun.*, 2015, **36**, 1458–1471.
22 G. Delaittre, M. Save and B. Charleux, *Macromol. Rapid Commun.*, 2007, **28**, 1528–1533.
23 R. Arshady, *Colloid Polym. Sci.*, 1992, **270**, 717–732.
24 N. P. Truong, J. F. Quinn, M. R. Whittaker and T. P. Davis, *Polym. Chem.*, 2016, **7**, 4295–4312.
25 J. Yeow and C. Boyer, *Adv. Sci.*, 2017, **4**, 1700137.
26 B. Karagoz, L. Esser, H. T. Duong, J. S. Basuki, C. Boyer and T. P. Davis, *Polym. Chem.*, 2014, **5**, 350–355.
27 M. Semsarilar, V. Ladmiral, A. Blanazs and S. Armes, *Langmuir*, 2012, **28**, 914–922.
28 M. Semsarilar and V. Abetz, *Macromol. Chem. Phys.*, 2020, **222**, 2000311.
29 T. Arita, M. Buback, O. Janssen and P. Vana, *Macromol. Rapid Commun.*, 2004, **25**, 1376–1381.
30 C.-Q. Huang and C.-Y. Pan, *Polymer*, 2010, **51**, 5115–5121.

31 W.-D. He, X.-L. Sun, W.-M. Wan and C.-Y. Pan, *Macromolecules*, 2011, **44**, 3358–3365.

32 W. Cai, W. Wan, C. Hong, C. Huang and C. Pan, *Soft Matter*, 2010, **6**, 5554–5561.

33 T. T. Dao, L. Vezenkov, G. Subra, V. Ladmiral and M. Semsarilar, *Polym. Chem.*, 2021, **12**, 113–121.

34 N. P. Truong, C. Zhang, T. A. Nguyen, A. Anastasaki, M. W. Schulze, J. F. Quinn, A. K. Whittaker, C. J. Hawker, M. R. Whittaker and T. P. Davis, *ACS Macro Lett.*, 2018, **7**, 159–165.

35 F. D'Agosto, J. Rieger and M. Lansalot, *Angew. Chem.*, 2020, **132**, 8444–8470.

36 M. J. Derry, L. A. Fielding and S. P. Armes, *Prog. Polym. Sci.*, 2016, **52**, 1–18.

37 Y. Pei and A. B. Lowe, *Polym. Chem.*, 2014, **5**, 2342–2351.

38 M. Semsarilar, V. Ladmiral, A. Blanazs and S. P. Armes, *Polym. Chem.*, 2014, **5**, 3466–3475.

39 W. M. Wan, X. L. Sun and C. Y. Pan, *Macromol. Rapid Commun.*, 2010, **31**, 399–404.

40 X. Zhang, J. Rieger and B. Charleux, *Polym. Chem.*, 2012, **3**, 1502–1509.

41 F. Huo, X. Wang, Y. Zhang, X. Zhang, J. Xu and W. Zhang, *Macromol. Chem. Phys.*, 2013, **214**, 902–911.

42 E. Jones, M. Semsarilar, P. Wyman, M. Boerakker and S. Armes, *Polym. Chem.*, 2016, **7**, 851–859.

43 G. G. du Sart, I. Vukovic, Z. Vukovic, E. Polushkin, P. Hiekkataipale, J. Ruokolainen, K. Loos and G. ten Brinke, *Macromol. Rapid Commun.*, 2011, **32**, 366–370.

44 I. Tokarev, R. Krenek, Y. Burkov, D. Schmeisser, A. Sidorenko, S. Minko and M. Stamm, *Macromolecules*, 2005, **38**, 507–516.

45 A. Knoll, R. Magerle and G. Krausch, *J. Chem. Phys.*, 2004, **120**, 1105–1116.

46 J. N. Albert and T. H. Epps III, *Mater. Today*, 2010, **13**, 24–33.

47 E. B. Gowd, M. Böhme and M. Stamm, *IOP Conf. Ser.: Mater. Sci. Eng.*, 2010, **14**, 012015.

48 W. Sriprom, M. James, S. Perrier and C. Neto, *Macromolecules*, 2009, **42**, 3138–3146.

49 N. A. Lynd and M. A. Hillmyer, *Macromolecules*, 2005, **38**, 8803–8810.

50 S. Park, J.-Y. Wang, B. Kim, J. Xu and T. P. Russell, *ACS Nano*, 2008, **2**, 766–772.

51 K. Fukunaga, H. Elbs, R. Magerle and G. Krausch, *Macromolecules*, 2000, **33**, 947–953.

52 E. B. Gowd, B. Nandan, M. K. Vyas, N. C. Bigall, A. Eychmüller, H. Schlörb and M. Stamm, *Nanotechnology*, 2009, **20**, 415302.

53 J. K. Bosworth, M. Y. Paik, R. Ruiz, E. L. Schwartz, J. Q. Huang, A. W. Ko, D.-M. Smilgies, C. T. Black and C. K. Ober, *ACS Nano*, 2008, **2**, 1396–1402.

54 C. Liedel, C. W. Pester, M. Ruppel, V. S. Urban and A. Böker, *Macromol. Chem. Phys.*, 2012, **213**, 259–269.

55 S. Sakurai, *Polymer*, 2008, **49**, 2781–2796.

56 A. Sidorenko, I. Tokarev, S. Minko and M. Stamm, *J. Am. Chem. Soc.*, 2003, **125**, 12211–12216.

57 S. H. Kim, M. J. Misner, T. Xu, M. Kimura and T. P. Russell, *Adv. Mater.*, 2004, **16**, 226–231.

58 J. G. Kennemur, *Macromolecules*, 2019, **52**, 1354–1370.

59 A. Boyde, F. A. Mccorkell, G. K. Taylor, R. J. Bomphrey and M. Doube, *Microsc. Res. Tech.*, 2014, **77**, 1044–1051.

60 B. Yu, J. W. Chan, C. E. Hoyle and A. B. Lowe, *J. Polym. Sci., Part A: Polym. Chem.*, 2009, **47**, 3544–3557.

61 D. J. Keddie, *Chem. Soc. Rev.*, 2014, **43**, 496–505.

62 S. Förster, M. Zisenis, E. Wenz and M. Antonietti, *J. Chem. Phys.*, 1996, **104**, 9956–9970.

63 M. Antonietti, S. Heinz, M. Schmidt and C. Rosenauer, *Macromolecules*, 1994, **27**, 3276–3281.

64 W. Zha, C. D. Han, D. H. Lee, S. H. Han, J. K. Kim, J. H. Kang and C. Park, *Macromolecules*, 2007, **40**, 2109–2119.

65 D. H. Lee, H. Cho, S. Yoo and S. Park, *J. Colloid Interface Sci.*, 2012, **383**, 118–123.

66 T. Xu, J. Stevens, J. Villa, J. T. Goldbach, K. W. Guarini, C. T. Black, C. J. Hawker and T. P. Russell, *Adv. Funct. Mater.*, 2003, **13**, 698–702.

67 S. Park, J.-Y. Wang, B. Kim and T. P. Russell, *Nano Lett.*, 2008, **8**, 1667–1672.

68 S. Park, B. Kim, J. Y. Wang and T. P. Russell, *Adv. Mater.*, 2008, **20**, 681–685.

69 E. J. Crossland, S. Ludwigs, M. A. Hillmyer and U. Steiner, *Soft Matter*, 2007, **3**, 94–98.

70 R. Olayo-Valles, S. Guo, M. Lund, C. Leighton and M. A. Hillmyer, *Macromolecules*, 2005, **38**, 10101–10108.

71 Z. Zhang, M. M. Rahman, C. Abetz, B. Bajer, J. Wang and V. Abetz, *Macromol. Rapid Commun.*, 2019, **40**, 1800729.

72 V. Abetz, *Macromol. Rapid Commun.*, 2015, **36**, 10–22.

73 M. Radjabian and V. Abetz, *Prog. Polym. Sci.*, 2020, **102**, 101219.

74 J. Brandrup, H. Immergut and A. Grulke, *Polymer handbook*, John Wiley & Sons, New York, 1999.

75 L. Oss-Ronen, J. Schmidt, V. Abetz, A. Radulescu, Y. Cohen and Y. Talmon, *Macromolecules*, 2012, **45**, 9631–9642.

76 M. Gallei, S. Rangou, V. Filiz, K. Buhr, S. Bolmer, C. Abetz and V. Abetz, *Macromol. Chem. Phys.*, 2013, **214**, 1037–1046.

77 A. Jung, S. Rangou, C. Abetz, V. Filiz and V. Abetz, *Macromol. Mater. Eng.*, 2012, **297**, 790–798.